Role of surface states in Auger neutralization of He^+ ions on Ag surfaces

A. Sarasola
Fisika Aplikatua I Saila, Unibertsitate Eskola Politeknikoa, UPV/EHU, Europa Plaza 1, 20018 Donostia, Spain

V. M. Silkin
Donostia International Physics Center (DIPC), Manuel de Lardizabal pasealekua 4, 20018 Donostia, Spain

A. Arnau
Materialen Fisika Saila, Kimika Fakultatea, UPV/EHU and Centro Mixto CSIC-UPV/EHU, 1072 Posta Kutxatila, 20080 Donostia, Spain

(Received 8 August 2006; revised manuscript received 28 November 2006; published 3 January 2007)

Recent measurements of He^+ ion fractions that survive to a whole scatterig event when they impinge on Ag surfaces have shown two different and interesting effects: (1) a notable difference of surviving ion fraction depending on which crystallographic face of the target surface is studied [Yu. Bandurin *et al.*, Phys. Rev. Lett. **92**, 017601 (2004)], and (2) an uncommonly high ion fraction in the very-low-energy range (tens of eV) [S. Wethekam *et al.*, Phys. Rev. Lett. **90**, 037602 (2003)]. Apart from the geometry, one of the differences between the surfaces of a crystal can be seen in the electronic structure: while the (111) surface has an occupied surface state near the Fermi level at the $\bar{\Gamma}$ point the (110) and (100) faces have not. Motivated by these facts, in this work we study the role that the occupied surface state plays on the Auger neutralization rate and we present an estimation of the ion fractions that survive for the different Ag faces.

DOI: 10.1103/PhysRevB.75.045104 PACS number(s): 79.20.Rf, 61.85.+p, 79.60.Bm

I. INTRODUCTION

The neutralization of a singly charged ion in front of a surface occurs when an electron from the solid occupies a hole in the ion, turning it into a neutral atom. Several kinds of neutralization processes can be distinguished: among them, resonant transfer and Auger neutralization processes. When the electronic state of the ion coincides in energy with the occupied conduction band states of the metal, the electron transfer is said to occur resonantly. Only one electron is involved in this process. However, when the final electronic state is far below the bottom of the valence band states in the solid, two electrons participate in the process. One is captured by the ion and the other one gets excited due to the potential energy gain of the first one. But this simple description of neutralization is not complete. The electron-electron interaction is, in fact, the ultimate reason for the Auger neutralization. Therefore, for a realistic description of these processes, a many-particle treatment of the system must be done. Presently, it is impossible to tackle this problem without doing approximations. In the literature, one finds numerous works devoted to the Auger neutralization. One of the earliest treatments was proposed by Hagstrum.[1,2] He measured the electron emission from some metals such as Cu, *W*, and Ni due to the neutralization of noble gas ions and proposed an exponential decay of the neutralization rate as a function of the distance. Since then, many theoretical works have approached the problem.[3–14,17] The development of experimental techniques as electron emission spectroscopy[18–21] and ion scattering spectroscopy[22–26] also contributes to a better understanding of the microscopic nature of the Auger neutralization process.

The physics involved in the bulk metal changes considerably when the symmetry is broken by a surface. In particular, periodicity of the wave functions in the z direction normal to the surface is no longer required and the resulting new boundary conditions for the wave functions give rise to the existence of electron states at energies forbidden in the bulk. Such states are called surface states. Among them, our interest is focused on Shockley states, also called crystal-induced surface states, which have their wave function localized at the surface. Its relative position with respect to the Fermi energy determines whether it is occupied or not. It is well established that occupied Shockley states exist at the $\bar{\Gamma}$ point of the surface Brillouin zone on the (111) surfaces of the noble metals.[27] It is not the case for other crystallographic orientations, like (100) and (110).

Recent experiments[28–30] have measured ion fractions from different crystallographic faces of the same material. In particular, Bandurin *et al.*[28] measured the ion fractions that survive to a whole scattering event for slow He^+ ions impinging on different Ag faces, and show that a notable difference of this ion fraction exists. Wethekam *et al.*[29] measured an uncommonly high number of ions surviving the scattering event for very low incident energies of He^+ ions on Ag (111). In this work we present results on Auger neutralization rates of He^+ ions on different Ag surfaces, as well as, an estimation of the ion fractions surviving to the neutralization. The paper is organized as follows: Sec. II, is devoted to theoretical aspects where we explain the different ingredients that compose the evaluation of the Auger neutralization rate: (i) the response function of the surface and (ii) the Auger matrix elements. Section III presents the results of the differential and total Auger rates, as well as, the surviving ion fractions. Finally, Sec. IV summarizes the most important conclusions of the work.

Atomic units (a.u.) are used ($e=m_e=\hbar=1$), unless stated otherwise. Vectorial magnitudes are represented by an arrow;

their moduli, however, by an absence of it. Due to the symmetry of the problem, we separate three-dimensional (3D) magnitudes in their parallel and normal to the surface components, thus $\vec{r} \equiv (\vec{\rho}, z)$, $\vec{q} \equiv (\vec{Q}, q_z)$, and $\vec{k} \equiv (\vec{K}, k_z)$.

II. THEORY

A. Auger neutralization rate

The Auger neutralization rate is defined as the probability per unit time of neutralizing an ion via the two-electron process schematically shown in Fig. 1. To approach the problem in a feasible way, we must distinguish the captured electron from the rest. Thus, the electrons in the conduction band can be labeled by their momentum $\vec{k}$ and the Auger rate is given by the sum of probabilities of the electrons in the band of going to a final bound state (s) of the ion:[14]

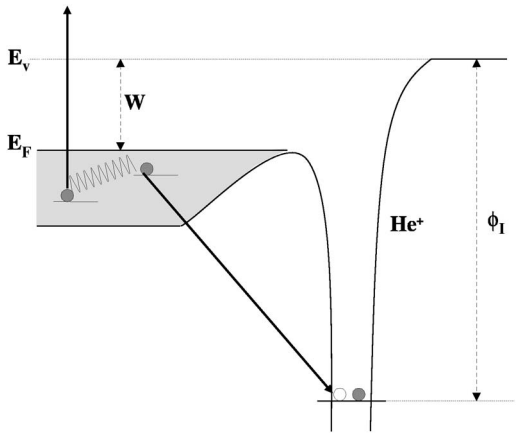

FIG. 1. Sketch of the Auger neutralization process. One electron from the conduction band of the metal is deexcited to an empty atomic level, giving rise to the excitation of another electron in the band. E_v and $E_F = \frac{1}{2}k_F^2$ are the vacuum level and Fermi energy, respectively. $W = E_v - E_F$ is the work function and ϕ_I the ionization potential of the He^+ ion.

$$\Gamma = \sum_{|\vec{k}| \leq k_F} \Gamma_k = -2 \sum_{|\vec{k}| \leq k_F} \int d\omega \int dz_1 \int dz_2 \int \frac{d\vec{Q}}{(2\pi)^2} \mathrm{Im}\{\chi(Q, z_1, z_2, \omega)\} \times A_{s\vec{k}}(Q, z_1) A^*_{\vec{k}s}(Q, z_2) \times \delta(\omega - (E_{\vec{k}} - E_s)). \quad (1)$$

Here, we do not distinguish among the different rates that should be considered due to the spin of the electrons.[15,16] The product of the Auger matrix elements $A_{s\vec{k}}(Q, z_1)$ and $A^*_{\vec{k}s}(Q, z_2)$ gives the probability of the electron to go from $\psi_{\vec{k}}$ to ψ_s state. These matrix elements are defined as follows:

$$A_{s\vec{k}}(Q, z_1) = \int dz \int d\vec{\rho} V(Q, z, z_1) e^{i\vec{Q}\vec{\rho}} \psi^*_{\vec{k}}(\vec{\rho}, z) \psi_s(\vec{\rho}, z), \quad (2)$$

where the Coulomb potential is Fourier transformed in two dimensions (2D) according to

$$v(\vec{r} - \vec{r}_1) = \frac{1}{|\vec{r} - \vec{r}_1|} = \int \frac{d\vec{Q}}{(2\pi)^2} e^{i\vec{Q}(\vec{\rho} - \vec{\rho}_1)} V(Q, z, z_1) \quad (3)$$

with

$$V(Q, z, z_1) = \frac{2\pi}{Q} e^{-Q|z - z_1|}. \quad (4)$$

Electronic excitations in the metal are described by the imaginary part of the density response function, $\mathrm{Im}\,\chi(Q, z_1, z_2, \omega)$, where $\chi(Q, z_1, z_2, \omega)$ represents the 2D Fourier transform of the density response function of the interacting electron system.[31] This magnitude accounts for the surface response to an external electric field giving rise to elementary one-particle (electron-hole pairs) and collective excitations (bulk and surface plasmons). The parallel momentum $\vec{Q}$ and the exchanged energy ω define the surface excitations, and thus, the available neutralization channels. At $Q = 0$ the energy required to excite bulk and surface plasmons is $\omega_p = \sqrt{4\pi n_0}$ (where n_0 is the average valence electron density in the metal) and $\omega_s = \omega_p / \sqrt{2}$, respectively. The minimum and maximum energy transfers correspond to the deexcitation of electrons from the bottom and the top of the valence band of the solid, respectively. Thus, $\Delta E_{\min} = \phi_I - W - E_F$ and $\Delta E_{\max} = \phi_I - W$, where ϕ_I is the ionization potential of the ion, W is the work function, and E_F is the Fermi energy. For the case of a He^+ ion in front of a silver surface, $\Delta E_{\min} \simeq 1.58\omega_p$ and $\Delta E_{\max} \simeq 2.2\omega_p$, where ω_p is the bulk plasmon frequency. Therefore, both electron-hole pair and plasmon excitations are possible.

The final state of the deexcited electron in the Auger neutralization is a bound state of the atom that is near the metal surface. To describe its electron wave function we use

$$\psi_s(\vec{r}) = \sqrt{\frac{\alpha^3}{\pi}} e^{-\alpha|\vec{r} - (0,0,z_0)|}, \quad (5)$$

where $\alpha = 1.6875$ a.u. and the position of the atom is $(0, 0, z_0)$ units displaced from the surface. The origin of the z coordinate is located at the top-most layer, unless it is otherwise indicated. The atomic wave function is not expected to be significantly perturbed at typical neutralization distances ($z_0 \sim 5$ a.u.) by the metal states, since the ground-state energy is well below the conduction band of silver.

B. Surface electronic states

In case of a semi-infinite medium, and concerning the occupied (below the Fermi energy) electron states, two types of levels are distinguished: bulk and surface states. Bulk states refer to those electrons located inside the solid that are not affected significantly by the symmetry breaking due to the presence of the surface. Surface states, however, as their name indicates, have their origin in the existence of a surface. Even if the generic "surface states" name includes different kinds of electronic states, we only deal with those induced by crystal potential at the surface, also called Shockley states.

The potential experienced by an electron as it approaches a surface is rather complicated. In the vacuum region far from the surface, at a distance z, the electron feels the classical image potential, $V_{\mathrm{im}}=-1/4(z-z_{\mathrm{im}})$, where z_{im} is the image plane position. However, deep inside the solid the crystal potential is dominant. The interface region potential is the most difficult to describe. From the simplest step potential to a self-consistent description of the ion-surface potential,[14] there exist many levels of approximation. We consider a slab scheme with a parametrized potential in the normal direction to the surface for the description of the surface barrier. The solution of the Schrödinger equation with the effective potential provides the corresponding electronic wave functions of the medium. This description accounts for the band structure in the direction normal to the surface and thus, provides a realistic description of the features derived due to the presence of a surface in the system.

We consider a metal slab of finite thickness a along the z direction with large vacuum regions at each side of width z_{vac}. In this model, the electrons can move freely in the plane parallel to the surface, while in the perpendicular coordinate they are bounded to an effective potential, $V_{\mathrm{eff}}(z)$. Thus, $\psi_{\vec{k}}$ wave functions take the form

$$\psi_{\vec{k}}(\vec{r}) \equiv \psi_{n,\vec{K}}(\vec{\rho},z) = \frac{1}{\sqrt{A}} e^{i\vec{K}\vec{\rho}} \phi_n(z), \tag{6}$$

where A is a normalization area in the x-y plane and $\phi_n(z)$ satisfies the Schrödinger equation

$$\left[-\frac{1}{2}\frac{d^2}{dz^2} + V_{\mathrm{eff}}(z) \right] \phi_n(z) = \epsilon_n \phi_n(z). \tag{7}$$

The 3D energy values are composed by a parallel and perpendicular component:

$$\epsilon_{n,\vec{K}} = \frac{K^2}{2m_n^*} + \epsilon_n, \quad n = 1,2,3, \ldots . \tag{8}$$

m_n^* is the effective mass of the electrons. In this calculation we use $m_n^*=1$ for all occupied bands. In the case of the surface state electrons, a realistic effective mass ($m_n^* \approx 0.44$) would reduce the phase space where it is occupied and thus, its contribution to the total rate. The effective potential is described by a one-dimensional model potential that reproduces the experimental values of the projected band structure perpendicular to the surface. A detailed description of this potential is given in Refs. 32 and 33. Using the slab geometry, the numerical evaluation of the wave functions is largely simplified if an adequate basis set is chosen to represent the metal electrons. Thus, we introduce a Fourier cosine series to represent the wave function perpendicular to the surface:

$$\phi_n(z) = \sum_{l=0}^{\infty} \left(\frac{g_l}{d} \right)^{1/2} a_l^{(n)} \cos\left(\frac{2l\pi z}{d} \right), \tag{9}$$

where

$$g_l = \begin{cases} 1, & l = 0, \\ 2, & l \neq 0, \end{cases} \tag{10}$$

$d=a+2z_{\mathrm{vac}}$ is the total thickness of the periodic system, and the origin is located at the center of the slab. Substituting Eq. (9) into Eq. (7) we obtain the following matrix version of Eq. (7):

$$\sum_{l'=0}^{\infty} M_{ll'} a_{l'}^{(n)} = \epsilon_n a_l^{(n)}, \quad l = 0,1,2,3, \ldots , \tag{11}$$

where $M_{ll'}$ matrix elements are the sum of the components corresponding to the kinetic energy and the effective potential:

$$M_{ll'} = M_{ll'}^{\mathrm{Kin}} + M_{ll'}^{\mathrm{eff}} \tag{12}$$

and

$$M_{ll'}^{\mathrm{Kin}} = \frac{1}{2}\left(\frac{2l\pi}{d} \right)^2 \delta_{l,l'}, \tag{13}$$

$$M_{ll'}^{\mathrm{eff}} = \frac{(g_l g_l')^{1/2}}{d} \int_0^d dz V_{\mathrm{eff}}(z) \cos\left(\frac{2l\pi z}{d} \right) \cos\left(\frac{2l'\pi z}{d} \right). \tag{14}$$

From the solution of Eq. (11) electron wave functions are obtained. Our interest is focused in those bulk and surface bands with energies below the Fermi level.

C. Crystallographic faces: Ag(100) and Ag(111)

The orientation of a crystal surface determines its structural and electronic properties. The cut of a three-dimensional crystal normal to (100), (110), and (111) crystallographic directions gives rise to crystal surfaces with the same Miller indexes. Similarly, a projection of three-dimensional bands along the direction normal to the surface is used to represent the surface electronic structure. Experimentally, these energy bands are determined by taking angle-resolved direct and inverse photoemission spectra[27] for occupied and unoccupied states, respectively. At (111) noble metal surfaces, there exists a partially occupied surface state band. In the (100) and (110) surfaces, however, no occupied surface states at $\bar{\Gamma}$ exist.

In this paper, the (100) and (111) faces of silver are studied. Their schematic surface band structures are represented in Fig. 2. As explained above, the main difference between (100) and (111) surface band structure is the existence of an

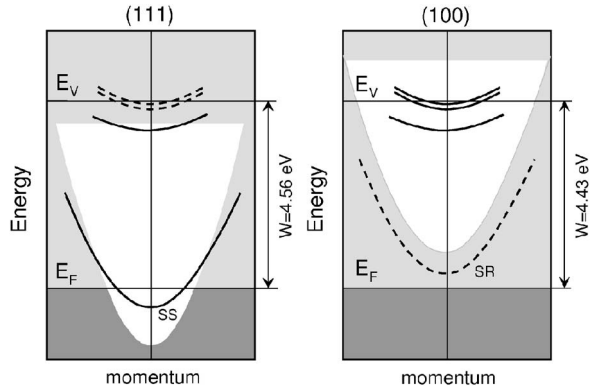

FIG. 2. Schematic representation of the projected band structures of Ag(111) and Ag(100) surfaces. Colored areas correspond to projected bulk electron states, while white ones show forbidden regions for them. Occupied and nonoccupied states are represented by dark- and light-colored areas, respectively. The surface state and surface resonance are labeled by SS and SR, respectively, and the bands depicted near the vacuum level, E_v, correspond to image states.

occupied crystal-induced surface state at $\epsilon_n=0.2023$ a.u. with respect to the bottom of the band at $K=0$ in the case of Ag(111) surface.

The geometrical differences between both faces are also important. We are interested in the relative space between the atoms, i.e., the area per atom or inverse of surface atomic density. In the case of (100) surface, the area per atom is $\Omega_{(100)}=\frac{1}{2}a^2$, whereas in the (111) case, $\Omega_{(111)}=\frac{\sqrt{3}}{4}a^2$. Therefore, (111) surface is more close-packed than (100). This factor will be used in the calculation of the ion trajectory to obtain an estimation of the ion fractions.

D. Response function

For a system of interacting electrons exposed to an external potential $v^{\text{ext}}(\vec{r},\omega)$, the induced charge density is

$$n^{\text{ind}}(\vec{r},\omega)=\int d\vec{r}'\chi(\vec{r},\vec{r}',\omega)v^{\text{ext}}(\vec{r}',\omega), \tag{15}$$

where $\chi(\vec{r},\vec{r}',\omega)$ is, by definition, the linear density response function.

In the random-phase approximation (RPA), the electron density induced by the external potential $v^{\text{ext}}(\vec{r},\omega)$, is approximated by the electron density induced in a noninteracting electron gas by the total field $v^{\text{ext}}(\vec{r},\omega)+v^{\text{ind}}(\vec{r},\omega)$:

$$\begin{aligned} n^{\text{ind}}(\vec{r},\omega) &= \int d\vec{r}'\chi^{\text{RPA}}(\vec{r},\vec{r}',\omega)v^{\text{ext}}(\vec{r}',\omega) \\ &= \int d\vec{r}'\chi^{0}(\vec{r},\vec{r}',\omega)\times[v^{\text{ext}}(\vec{r}',\omega)+v^{\text{ind}}(\vec{r}',\omega)], \end{aligned} \tag{16}$$

which is equivalent to

$$\chi^{\text{RPA}}(\vec{r},\vec{r}',\omega)=\chi^{0}(\vec{r},\vec{r}',\omega)+\int d\vec{r}_1\int d\vec{r}_2\chi^{0}(\vec{r},\vec{r}_1,\omega)\times v(\vec{r}_1-\vec{r}_2)\chi^{\text{RPA}}(\vec{r}_2,\vec{r}',\omega), \tag{17}$$

where $\chi^0(\vec{r},\vec{r}',\omega)$ is the density response function of noninteracting electrons:

$$\chi^{0}(\vec{r},\vec{r}',\omega)=2\sum_{n,\vec{K},n',\vec{K}'}\frac{\psi_{n,\vec{K}}(\vec{r})\psi^{*}_{n',\vec{K}'}(\vec{r})\psi_{n',\vec{K}'}(\vec{r}')\psi^{*}_{n,\vec{K}}(\vec{r}')}{\epsilon_{n,\vec{K}}-\epsilon_{n',\vec{K}'}+(\omega+i\eta)}\times[\theta(E_F-\epsilon_{n,\vec{K}})-\theta(E_F-\epsilon_{n',\vec{K}'})], \tag{18}$$

where $\psi_{n,\vec{K}}(\vec{r})$ represents one-electron states of energy $\epsilon_{n,\vec{K}}$, and $v(\vec{r}_1-\vec{r}_2)$ is defined by Eq. (3).

Due to the two-dimensional translational invariance along the surface, i.e.,

$$\chi(\vec{r},\vec{r}',\omega)=\chi(\vec{\rho}-\vec{\rho}',z,z',\omega), \tag{19}$$

all magnitudes are more conveniently described using the 2D Fourier transform. Thus, equivalent equations to (15) and (17) can be written for the case of a surface:

$$n^{\text{ind}}(Q,z,\omega)=\int dz'\chi(Q,z,z',\omega)v^{\text{ext}}(Q,z',\omega) \tag{20}$$

and

$$\chi(Q,z,z',\omega)=\chi_0(Q,z,z',\omega)+\frac{2\pi}{Q}\times\int dz_1\int dz_2\chi_0(Q,z,z_1,\omega)e^{-Q|z_1-z_2|}\times\chi(Q,z_2,z',\omega). \tag{21}$$

In practice, to obtain the surface response function χ, we must solve Eq. (21). We begin constructing the independent electron response function $\chi_0(Q,z,z',\omega)$ by using the one-electron wave functions calculated with the effective potential. Using the slab geometry, the response functions $\chi_0(Q,z,z',\omega)$ and $\chi(Q,z,z',\omega)$ can be expanded in a sine-cosine series.[31]

E. Auger matrix elements

In this section, we describe the mathematical procedure used to obtain the Auger matrix elements required in the neutralization rate calculation. As the initial and final states are required to be orthogonal to avoid spurious contributions, new Auger matrix elements are defined as

$$B_{snK}=A_{snK}-S_{snK}A_{ss}, \tag{22}$$

where

$$A_{snK}(Q,z_1)=\langle\psi_s|V(Q,z,z_1)e^{i\vec{Q}\vec{\rho}}|\psi_{n,\vec{K}}\rangle, \tag{23}$$

$$S_{snK}=\langle\psi_s|\psi_{n,\vec{K}}\rangle, \tag{24}$$

$$A_{ss}(Q,z_1) = \langle \psi_s | V(Q,z,z_1) e^{i\vec{Q}\vec{\rho}} | \psi_s \rangle, \quad (25)$$

and $V(Q,z,z_1)$ is the 2D Fourier transform of the Coulomb potential defined in Eq. (4). The evaluation of such integrals requires to take into account their multicentered nature. The integrals are long and tedious, but regardless the results are analytic.

F. Ion fractions and trajectory

In order to obtain ion fractions, the distance-dependent Auger rates are needed. Although the treatment of the neutralization rate is strictly valid for static projectiles, for very low ion velocities the perturbation introduced due to the ion motion can be considered as quasi-adiabatic. For low incident velocities, ion trajectories are simulated taking into account the incidence conditions and the ion-surface potential. Ideally, an *ab initio* potential that considers the ion-surface system as a whole should be used. We, as a first approximation, consider the Ziegler-Biersack-Littmark (ZBL) (Ref. 34) potential, which accounts for the purely repulsive part of the interaction between the ion and the surface. Thus, the ion trajectory is given by

$$z(t) = \int_{-\infty}^{t} dt' \sqrt{\frac{2}{M}[E_0 \sin^2 \phi - U_{\mathrm{ZBL}}(z(t'))]}, \quad (26)$$

where M is the projectile mass, E_0 and ϕ are the incident energy and angle, and $U_{\mathrm{ZBL}}(z)$ is the above-mentioned potential.

The time dependence of the ion fraction that survives to the scattering event is governed by a rate equation:

$$\frac{d}{dt}P^+ = \Gamma_L P^0 - \Gamma_C P^+, \quad (27)$$

where all the processes that have certain probability to occur should be included on Γ_L (in case the ion loses an electron) or Γ_C (in case the ion captures an electron). In our particular case, the energy levels of the He^+ ion are much lower than those of the conduction band of the silver. This feature has two consequences: (1) loss processes are much less probable than capture processes ($\Gamma_C \gg \Gamma_L$) and (2) the probability of capturing an electron resonantly for a static ion is negligibly small and thus the capture rate ($\Gamma_C = \Gamma_C^{\mathrm{Aug}} + \Gamma_C^{\mathrm{resonant}}$) is dominated by the capture via the Auger neutralization process. In these conditions the rate equation yields

$$\frac{d}{dt}P^+ \simeq -\Gamma_C^{\mathrm{Aug}} P^+. \quad (28)$$

Then the ion survival probability is given by

$$P^+ = \exp\left\{ -\int_{-\infty}^{\infty} dt \Gamma^{\mathrm{Aug}}(t) \right\} = \exp\left\{ -2\int_{z_0}^{z_{\max}} \frac{\Gamma^{\mathrm{Aug}}(z)dz}{\sqrt{\frac{2}{m}[E_0 \sin^2 \phi - U_{\mathrm{ZBL}}(z)]}} \right\}. \quad (29)$$

Here, the trajectory is considered to be symmetric with respect to z_0, the turning point of the trajectory.

III. RESULTS

The value of the neutralization rate of an ion at a certain distance from the surface is determined by the two main components that take part in the process, described in Eq. (1): the Auger matrix elements, $B_{snK}(Q,z_1)$, and the imaginary part of the surface response function, Im $\chi(Q,z_1,z_2,\omega)$. In this section, our main purpose is to understand the role played on the Auger rate and the surviving ion fractions by the occupied surface state in the (111) surface of silver. In order to do so, we analyze, one by one, the elements included in Eq. (1) and compare them for both surfaces: Ag(100) and Ag(111).

A. Auger matrix elements and surface response function

The penetration of the electron wave function of solid into the vacuum region is a key factor in the Auger matrix elements, as the wave function that corresponds to the atomic electron does not significantly change for a given ion-surface distance ($z_0 > 3$ a.u.). The bulk electrons are mainly localized inside the solid, i.e., only an evanescent tail of electronic density is extended out of the solid, in the vacuum side. This implies that the Auger matrix element will not be large. However, the charge distribution of the Shockley surface state is centered on the surface and the matrix element between surface state and atomic wave functions will certainly be higher than in the case of bulk states. This is, precisely, what can be observed in Fig. 3, where we show the spatial dependence of the Auger matrix elements for some electronic states with energies near the Fermi level for both surfaces, Ag(100) (in the top panel) and Ag(111) (in the bottom panel).

The matrix element corresponding to the occupied surface state in Ag(111) takes values much higher than any other. As the matrix elements represent a probability amplitude, the real effect in the rate equation is of more than one order of magnitude in the probability. The same result is observed in Fig. 4.

Here, we show the Auger matrix element values as a function of their perpendicular energy (ϵ_n) in the conduction band for fixed values of Q and z ($Q=0.5$ a.u. and $z=5$ a.u.). As we go up in the band energy, we observe that the electron wave functions extend more in the vacuum side giving rise to larger matrix elements. The values corresponding to bulk states in both surfaces are quite similar. However, the surface state, which has $\epsilon_n = 0.2023$ a.u., yields, by far, the largest value.

The second important ingredient to understand the role of the surface state in the Auger neutralization of an ion is the surface response function. The imaginary part of the surface response function accounts for the probability of creating an elementary excitation at the surface with momentum Q and energy transfer ω. In the following figures, we analyze the behavior of this magnitude for Ag(100) and Ag(111). Three different positions (inside the solid, at the surface and outside the solid) of a probe particle (represented by a filled square)

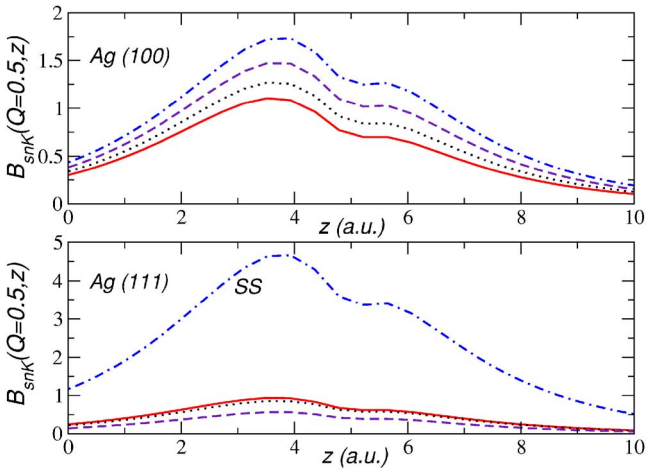

FIG. 3. (Color online) Auger matrix elements as a function of the perpendicular coordinate z for $Q=0.5$ a.u. and for four different electronic states of the conduction band of silver. In the top panel, the values of B_{snK} for Ag(100) surface are represented: solid, dotted, dashed, and dot-dashed lines are used for $\epsilon_n=0.1535$ a.u., $\epsilon_n=0.1689$ a.u., $\epsilon_n=0.1846$ a.u., and $\epsilon_n=0.2001$ a.u. energy values, respectively; in the bottom panel, B_{snK} values for Ag(111) surface: solid, dotted, dashed, and dot-dashes lines are used for $\epsilon_n=0.1687$ a.u., $\epsilon_n=0.1779$ a.u., $\epsilon_n=0.1845$ a.u., and $\epsilon_n=0.2023$ a.u. energy values, respectively, the last one corresponding to the surface state. The energy values are according to the bottom of the valence band. ($E_F=0.2046$ a.u.)

are chosen to analyze the spatial dependence of the imaginary part of the surface response function in Fig. 5. We also fix the exchanged momentum and energy values to $Q=0.5$ a.u. and $\omega=2\omega_p$.

As one can observe in the figure, when the probe particle is located inside the solid ($z=-6$ a.u.) (bottom panel) and at the surface ($z=0$ a.u.) (middle panel) the behavior of Im $\chi(Q,z,z',\omega)$ is mainly local, which means that the minima of the function correspond to the $z=z'$ position.

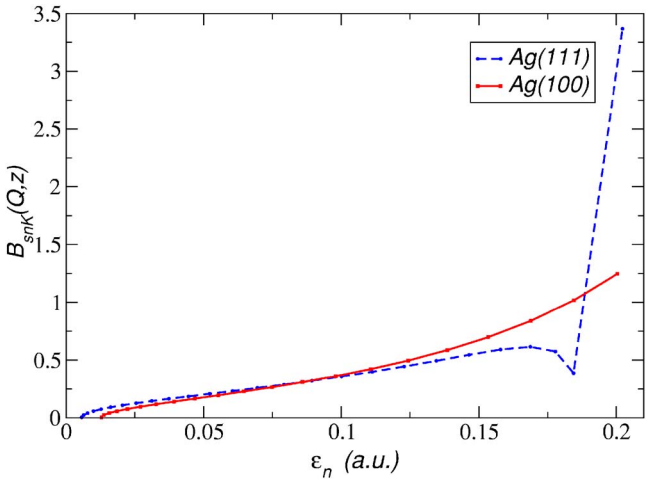

FIG. 4. (Color online) Auger matrix elements as a function of the perpendicular energy of the valence band for $Q=0.5$ a.u. and $z=5$ a.u. The energy range goes from the bottom of the valence band ($\epsilon_n=0$ a.u.) to the Fermi energy.

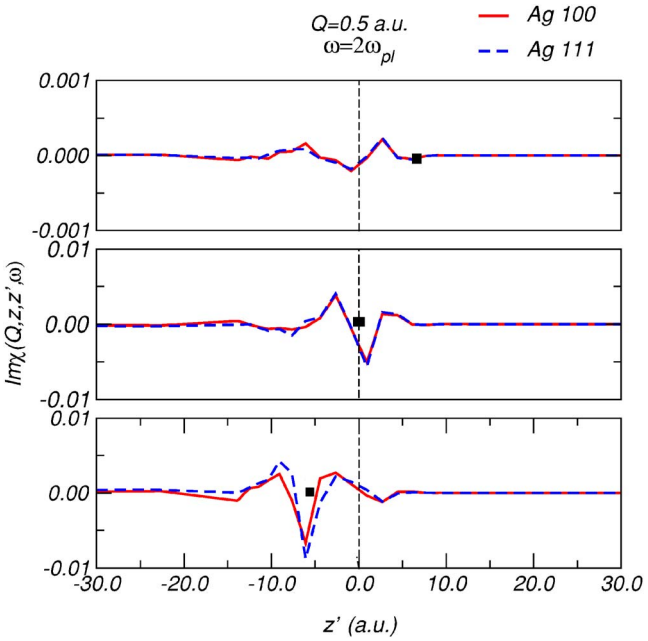

FIG. 5. (Color online) Imaginary part of the surface density response function for $Q=0.5$ a.u. and $\omega=2\omega_p$. The z coordinate has been fixed for three positions: $z=6$ a.u., $z=0$ a.u., and $z=-6$ a.u. that correspond to the top, middle, and bottom panels, respectively.

However, this is not the case when the probe particle is moved to the vacuum side of the system ($z=6$ a.u.) (top panel). Then the response of the system to an external probe particle is nonlocal, i.e., it remains being localized at the surface while the particle is outside.

While the most significant values of the response function are located at the surface and the bulk regions of the solid, the neutralization of the ion takes place some atomic units away from the surface. Here, the probability of creating an excitation decreases rapidly. Moreover, at distances between 3 and 10 a.u. from the surface, the difference between both surfaces can hardly be estimated. This means that the presence of an occupied surface state does not change significantly the collective response of the solid to an external perturbation. However, the responses for both surfaces are not exactly equal. In Fig. 6, we zoom out this region and represent, for $z=z'=5$ a.u., the surface response value for every exchanged energy ω from the bottom to the top of the conduction band. In the whole range of transferred energy the response of the (111) surface is approximately 10% higher than in the (100) case.

B. Differential and total rates

The consecutive integrals of the differential magnitudes in the different variables give rise to the total rates of neutralization. Thus, the evaluation of these integrals leads to quantities that can be measured experimentally. In our case, only the ion fractions that are deduced from the total rate of neutralization can be compared with the experimental results.

In this section, we are interested in following the influence of an occupied surface state at the Ag(111) surface as we make the different integrals. For this, we rewrite Eq. (1)

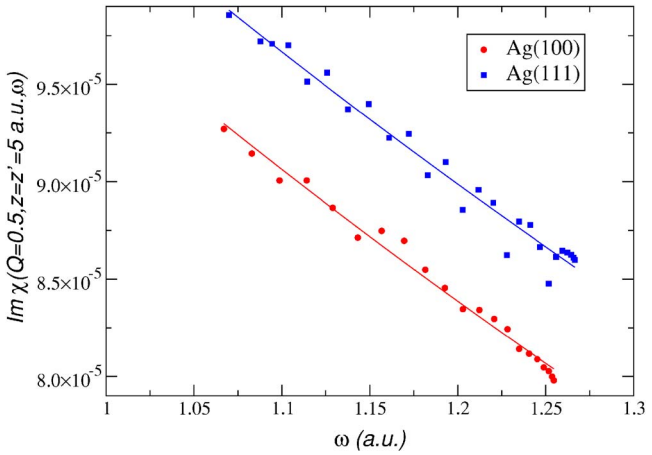

FIG. 6. (Color online) Imaginary part of the response function as a function of the exchanged energy for Ag(100) and Ag(111) surfaces. The other variables have been fixed to $z=z'=5$ a.u. and $Q=0.5$ a.u.

to understand the notation employed in the following figures,

$$\Gamma_{\text{tot}}(z_0) = \sum_{\epsilon_n} \Gamma_n = \sum_{\epsilon_n} \int_0^{\sqrt{2(E_F-\epsilon_n)}} 2\pi K dK \Gamma_{n,K}, \qquad (30)$$

where the index n indicates the conduction band states in the direction perpendicular to the surface, Γ_n refers to the differential rate in the energy perpendicular to the surface, and $\Gamma_{n,K}$ is the double differential rate with respect to the perpendicular energy and parallel momentum:

$$\Gamma_{n,K} = -2\left[\int dz_1 \int dz_2 \int \frac{d\vec{Q}}{(2\pi)^2} B_{snK}(Q,z_1) B^*_{nKs}(Q,z_2) \times \text{Im}\,\chi(Q,z_1,z_2,\omega)\right]. \qquad (31)$$

This double differential magnitude is shown in Fig. 7 for three different fixed values of K and for 5 a.u. ion-surface

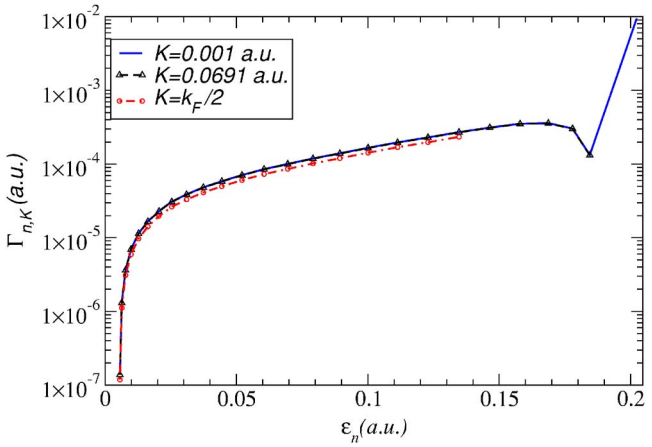

FIG. 7. (Color online) Integrand of Eq. (30) for the energy values of conduction band states and three fixed values of K: almost 0, the limit value of the occupied surface state, and $k_F/2$. These values are calculated for Ag(111) and an ion-surface distance of 5 a.u.

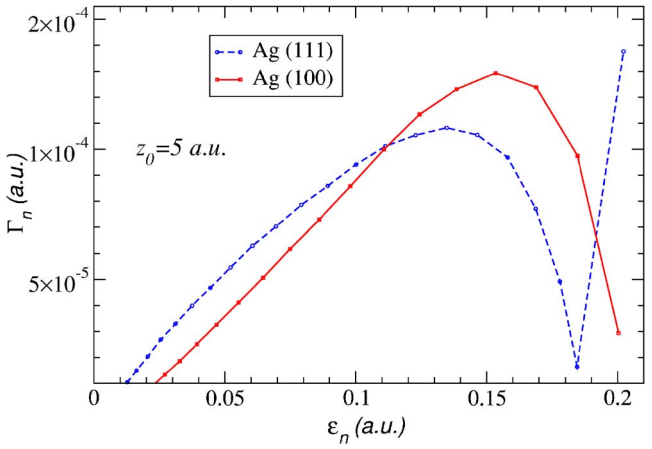

FIG. 8. (Color online) Partial contribution to the rate of neutralization from states in the conduction band as a function of their energy. The energy is referred to the bottom of the band. The ion-surface distance is 5 a.u.

distance. The chosen K values are $K \simeq 0$, the limit value of the occupied surface state, and $K=k_F/2$. In the former case, and as $0<E=\epsilon_n+\frac{K^2}{2}<E_F$ must be filled, the integral in ϵ_n is done for every state in the conduction band, or what is the same, the surface state dispersion band is below the Fermi energy and thus, corresponds to an occupied state. The second K value, however, corresponds to the K limit value where the surface state leaves being occupied. Among all the states, the intrinsic surface state stands out clearly. The contribution to the rate of this state is more than one order of magnitude higher than the magnitude of the contribution of the bulk states. This is mainly due to the Auger matrix elements, as obtained in the previous section of results.

In Fig. 8 the partial rates as a function of the band energy (measured from the Fermi level) are shown for Ag(100) and Ag(111). The relative importance of states at the bottom of the band increases after K summation is done. Among these latter states, the surface state still has a remarkable role in the partial rate, even if its effect results reduced as the total rate values are approached.

Finally, when the sum over the partial rates corresponding to different perpendicular energies is done, the total rates of neutralization are obtained. In Fig. 9 we show the results of this magnitude for different ion-surface distances. The rates for Ag(111) and Ag(100) surfaces decrease exponentially with the distance and their values differ approximately by a 30%.

Thus, one can conclude that the surface state enhances (111) neutralization rate values compared to those corresponding to the (100) surface, as can be seen in Fig. 9.

C. Ion fractions

The direct comparison with the experimental data must be done deriving from the neutralization rates the ion fractions that survive to the whole scattering event as described in Sec. II F. In this section, we compare our results with two recent experimental data sets.

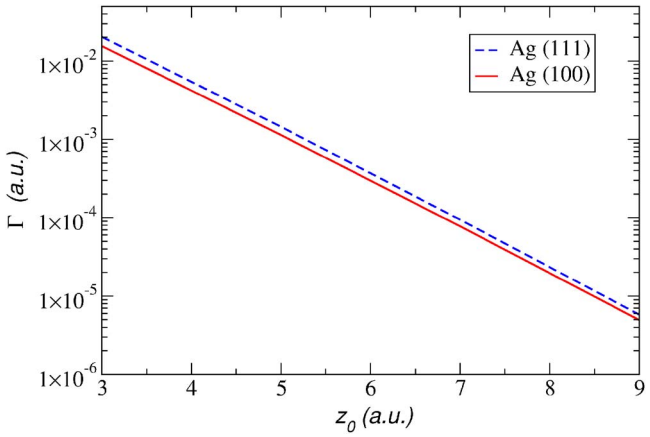

FIG. 9. (Color online) Total neutralization rates of He^+ ions on Ag(111) (dashed lines) and Ag(100) (solid lines) surfaces as a function of the ion-surface distance.

In the first one, He^+ ions are scattered on a Ag(111) surface for a fixed value of the scattering angle, $\phi=1.35°$, and the energy of incidence is varied in the range of 0.5 keV $<E_0<14$ keV. Hence, in the results shown in Fig. 10, the perpendicular energy is of the order of eV and grazing scattering conditions are obtained. The remarkable feature of these data, measured by Wethekam *et al.*,[29] is the low energy behavior. They found that, around $E_0=6$ keV, the ion fraction approaches a minimum and below this energy, the number of surviving ions increases considerably.

Our calculation reproduces rather well the pronounced increase of the number of surviving ions for decreasing incident energy, as can be observed in Fig. 10. This sudden growth is explained by means of a larger distance of maximum approach and thus, a much lower probability of being neutralized as energy decreases.

The effect of changing the crystallographic orientation is investigated in the second experimental data set, presented in Fig. 11. Bandurin *et al.*[28] measured the He^+ ion fractions outgoing from Ag(111) and Ag(110) surfaces. They show that the results on Ag(110) are about an order of magnitude higher than those in Ag(111).

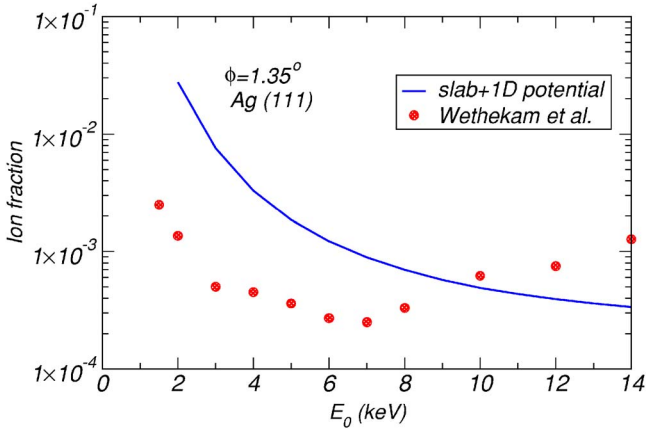

FIG. 10. (Color online) He^+ ion fraction as a function of the incident energy for scattering on Ag(100) surface. The experimental results of Wethekam *et al.*[29] are represented by circles while our simulation is given by a solid line.

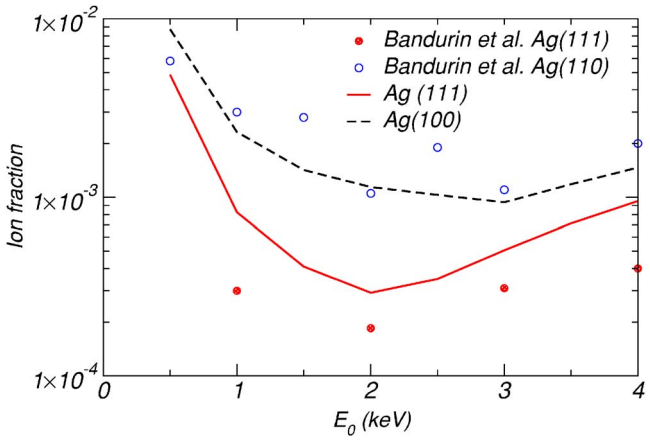

FIG. 11. (Color online) He^+ ion fraction as a function of the incident energy, for a fixed angle of incidence, $\phi=3.5°$. Solid and dashed lines correspond to theoretical calculations and full and empty circles to experimental measurements (Refs. 28 and 35).

Our calculation includes results on ion fractions for Ag(111) and Ag(100) surfaces. Thus, the calculations for the Ag(100) face allows us to extract a conclusion on the face dependence of ion fractions, since all the occupied states on (100) and (110) faces are bulk like at $\bar{\Gamma}$.

The comparison between the experimental and theoretical results on Ag(111) shows a good agreement. The position of the minimum is correctly simulated and the overall behavior is qualitatively well reproduced. As was shown in Fig. 9, the rates of neutralization for Ag(100) and Ag(111) surfaces differ approximately by 30% for the whole range of ion-surface distances. These differences cause almost an order of magnitude of change in the ion fractions.

IV. CONCLUSIONS

In this paper we present results obtained for the Auger neutralization rates and the ion fraction surviving the scattering of He^+ ions on different silver surfaces. We explain the difference between the ion fraction after He^+ neutralization on Ag(111) and Ag(100) as due to the contribution of the occupied surface state present in Ag(111) and not in Ag(100). A thorough theoretical analysis permits us to understand the contribution of the surface state to the two main factors determining the value of the Auger neutralization rate, i.e., the matrix element and the surface response function that contains all the many-body effects. We find that the surface state plays a role in determining the value of the matrix element but not that of the surface response. Therefore, we can assess that it is not a many-body effect.

A comparison with the experimental data has been done for the ion fraction results presented by two different groups. The overall qualitative agreement with these data is good. We reproduce the behavior at low incident energies. The use of a repulsive potential for the trajectory simulations, results sufficient to obtain the sudden increase of the ion fraction at very low incident energies. The presence of an occupied surface state in the Ag(111) surface is the main reason to exist an order of magnitude of difference on the number of sur-

viving ions for the distinct faces, and thus, we can conclude that the surface state at the center of the Brillouin zone has an active role in the neutralization of ions scattered in such face.

ACKNOWLEDGMENTS

We acknowledge the partial support from the University of the Basque Country (Grant No. 9/UPV 00206.215-13639/2001), the Departamento de Educación, Universidades e Investigación del Gobierno Vasco, the Spanish Ministerio de Ciencia y Tecnología (MCyT) (Grant No. FIS2004-06490-C03-01), and the European Community 6th Network of Excellence NANOQUANTA (Grant No. NMP4-CT-2004-500198).

[1] H. D. Hagstrum, Phys. Rev. **96**, 325 (1954).
[2] H. D. Hagstrum, Phys. Rev. **96**, 336 (1954).
[3] R. Hentschke, K. J. Snowdon, P. Hertel, and W. Heiland, Surf. Sci. **173**, 565 (1986).
[4] K. J. Snowdon, R. Hentschke, A. Närman, and W. Heiland, Surf. Sci. **173**, 581 (1986).
[5] R. K. Janev and N. N. Nedeljković, J. Phys. B **18**, 915 (1985).
[6] A. A. Almulhem and M. D. Girardeau, Surf. Sci. **210**, 138 (1989).
[7] J. M. Schins, R. B. Vrijen, W. J. van der Zande, and J. Los, Surf. Sci. **280**, 145 (1993).
[8] T. Fondén and A. Zwartkruis, Surf. Sci. **269/270**, 601 (1992).
[9] A. Zwartkruis and T. Fondén, Surf. Sci. **290**, 134 (1993).
[10] T. Fondén and A. Zwartkruis, Phys. Rev. B **48**, 15603 (1993).
[11] N. Lorente, R. Monreal, and M. Alducin, Phys. Rev. A **49**, 4716 (1994).
[12] N. Lorente and R. Monreal, Surf. Sci. **370**, 324 (1997).
[13] N. Lorente, M. A. Cazalilla, J.-P. Gauyacq, D. Teillet-Billy, and P. M. Echenique, Surf. Sci. **411**, L888 (1998).
[14] M. A. Cazalilla, N. Lorente, R. Diez Muiño, J. P. Gauyacq, D. Teillet-Billy, and P. M. Echenique, Phys. Rev. B **58**, 13991 (1998).
[15] M. Alducin, R. Díez Muiño, and J. I. Juaristi, Phys. Rev. A **70**, 012901 (2004).
[16] M. Alducin, J. I. Juaristi, R. Díez Muiño, M. Rösler, and P. M. Echenique, Phys. Rev. A **72**, 024901 (2005).
[17] D. Valdés, J. M. Blanco, V. A. Esaulov, and R. C. Monreal, Phys. Rev. Lett. **97**, 047601 (2006).
[18] P. Varga, W. Hofer, and H. Winter, Surf. Sci. **117**, 142 (1982).
[19] P. A. Zeijlmans van Emmichoven, P. A. A. F. Wouters, and A. Niehaus, Surf. Sci. **195**, 115 (1988).
[20] F. W. Meyer, S. H. Overbury, C. C. Havener, P. A. Zeiljmans van Emmichoven, J. Burgdörfer, and D. M. Zehner, Phys. Rev. A **44**, 7214 (1991).
[21] H. H. Brongersma and T. M. Buck, Surf. Sci. **53**, 649 (1975).
[22] W. Heiland and E. Taglauer, Nucl. Instrum. Methods **132**, 535 (1976).
[23] H. Akazawa and Y. Murata, Phys. Rev. B **39**, 3449 (1989).
[24] R. Souda, W. Hayami, T. Aizawa, W. Hayami, and S. Otani, Phys. Rev. B **42**, 7761 (1990).
[25] R. Souda, W. Hayami, T. Aizawa, S. Otani, and Y. Ishizawa, Phys. Rev. B **46**, 7315 (1992).
[26] H. Winter, J. Phys.: Condens. Matter **8**, 10149 (1996).
[27] A. Goldmann, V. Dose, and G. Borstel, Phys. Rev. B **32**, 1971 (1985).
[28] Yu. Bandurin, V. A. Esaulov, L. Guillemot, and R. C. Monreal, Phys. Rev. Lett. **92**, 017601 (2004).
[29] S. Wethekam, A. Mertens, and H. Winter, Phys. Rev. Lett. **90**, 037602 (2003).
[30] S. Wethekam and H. Winter, Phys. Rev. Lett. **96**, 207601 (2006).
[31] V. M. Silkin, J. M. Pitarke, E. V. Chulkov, and P. M. Echenique, Phys. Rev. B **72**, 115435 (2005).
[32] E. V. Chulkov, V. M. Silkin, and P. M. Echenique, Surf. Sci. **391**, L1217 (1997).
[33] E. V. Chulkov, V. M. Silkin, and P. M. Echenique, Surf. Sci. **437**, 330 (1999).
[34] J. F. Ziegler, J. P. Biersack, and U. Littmark, *The Stopping and Range of Ions in Solids* (Exeter: Pergamon, New York, 1985).
[35] R. C. Monreal, L. Guillemot, and V. A. Esaulov, J. Phys.: Condens. Matter **15**, 1165 (2003).